Supplementary Information (SI) for Journal of Materials Chemistry A.
This journal is © The Royal Society of Chemistry 2024

Supporting Information

High-voltage Symmetric Supercapacitors Developed by Engineering $DyFeO_3$ Electrodes and Aqueous Electrolytes

Mohasin Tarek, Ferdous Yasmeen, and M. A. Basith*

Nanotechnology Research Laboratory, Department of Physics,
Bangladesh University of Engineering and Technology, Dhaka-1000, Bangladesh.

Sample preparation

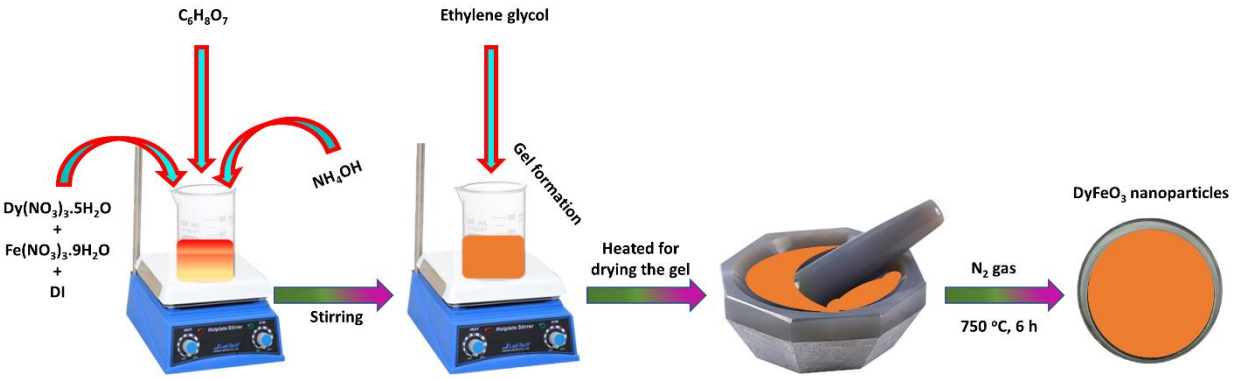

Fig. S1 *Schematic representation of the synthesis procedure of $DyFeO_3$ nanoparticles by sol-gel technique.*

Working electrode preparation

For three-electrode system

In both the three-electrode and symmetric two-electrode setups, an electrolyte comprising 0.5 M Na_2SO_4 in aqueous and hybrid solutions was employed. Fig. S2 illustrates the schematic representation of the preparation of the electrode slurry and the electrochemical arrangement for the three-electrode system. Within the three-electrode system, the reference electrode included an Ag/AgCl electrode immersed in a saturated KCl solution, while a counter electrode consisted of a platinum wire. For the preparation of the working electrode, 20 mg of the synthesized $DyFeO_3$ nanoparticles, serving as the active material (90 wt%), were sonicated with 2.22 mg of polyvinylidene fluoride (PVDF; 10 wt%) as a binder and 200 µL of N-methyl-2-pyrrolidone (NMP) as a solvent for 3 hours. This procedure resulted in a homogeneous slurry of the electrode material. The slurry was then evenly coated onto a graphite rod, which had a surface area of 0.28 cm^2. Subsequently, the modified graphite rod was subjected to a 12-hour drying process at 80 °C and was utilized as the working electrode in the three-electrode cell.

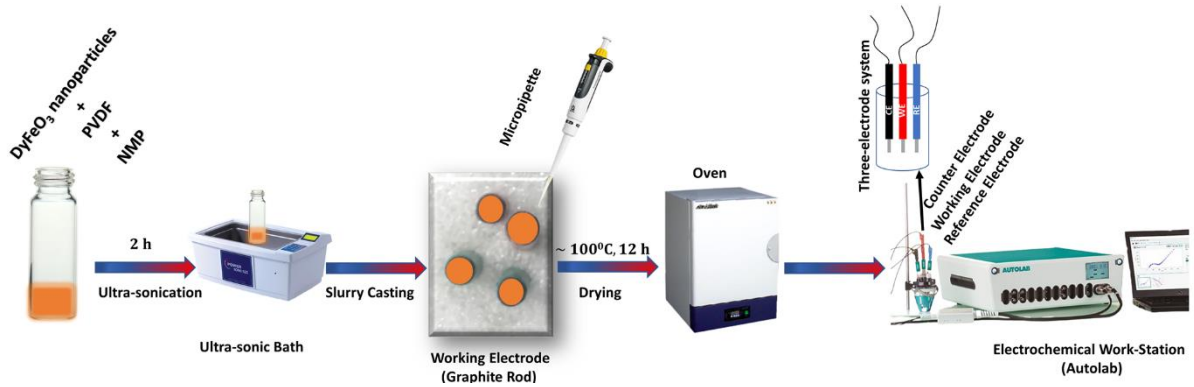

Fig. S2 *Schematic illustration of the preparation of electrode slurry and the configuration of the electrochemical setup.*

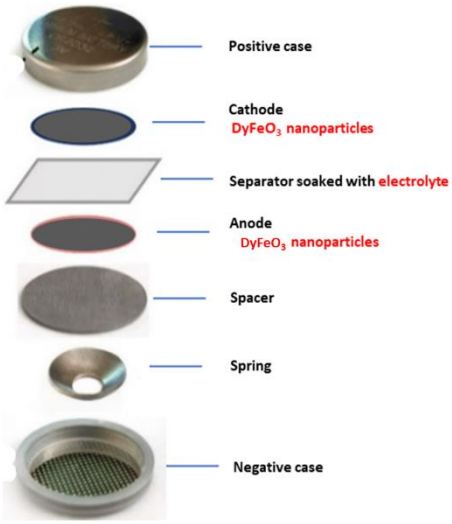

Coin cell arrangement

Coin cell sealed machine

Sealed coin cell

Fig. S3 *Schematic representation of the fabrication process of coin cell supercapacitor.*

Mathematical analysis

Electrochemical Measurement

Specific capacitance in the three-electrode system:

To calculate the capacitance (C_{cell} in F), and specific capacitance (C_{sp} in F g^{-1} unit) from the CV and GCD in the three-electrode system (or half cells), we employed Equation 1 and 2, respectively [1,2].

$$C_{sp} = \frac{\int J\,\Delta t}{2\nu\Delta V} \tag{1}$$

$$C_{sp} = \frac{J\Delta t}{\Delta V} \tag{2}$$

Where J, m, Δt, ΔV and ν stand for current density, mass of active material, time to discharge, potential window, and scan rate, respectively.

Specific capacitance in the symmetric two-electrode system:

To calculate the capacitance (C_{cell} in F), we employed Equation 3.

$$C_{cell} = \frac{I\Delta t}{\Delta V} \tag{3}$$

Where I, Δt, and ΔV stand for current, time to discharge, and potential window, respectively. The capacitance (C_{cell}) that arises when a voltage is applied between the two electrodes can be represented using the following formula:

$$\frac{1}{C_{cell}} = \frac{1}{C_+} + \frac{1}{C_-} \tag{4}$$

Here, C_{cell}, C_+, and C_- represent the capacitance (measured in Farads) of the resultant device or cell, the positive electrode, and the negative electrode, respectively. Upon obtaining the capacitance (C_{cell}) from the GCD profile using Equation 4, in a symmetric system where both positive and negative electrodes exhibit similar morphological and electronic characteristics ($C_+ = C_-$), the determination of cell capacitance (C_{cell}) outlined in Equation 5

$$C_{cell} = \frac{C}{2} \tag{5}$$

where $C = C_+ = C_-$. The electrode capacitance is calculated using the following Equation.:

$$C = 2 \times C_{cell} \tag{6}$$

In the field of electrochemical supercapacitors, to compare different electrode materials, it is a customary practice to assess the specific capacitance (C_{sp}). This parameter is linked to the

capacitance of an individual electrode and is denoted in F g^{-1}. Therefore, through the division of Equation 6 by the mass of a single electrode m, we can employ Equation 7.

$$C_{sp} = \frac{2 \times C_{cell}}{m} \tag{7}$$

Where *m* (g) is the mass of the single electrode. For a symmetric system, the specific capacitance of the single electrode (C_{sp}) is given by:

$$C_{sp} = \frac{4C_{cell}}{M} \tag{8}$$

The symbol *'M'* signifies the total mass of the active materials in both electrodes, equating to twice the *'m'* value as each electrode carries an identical weight. The factor of 4 functions as a correction, aligning the cell capacitance and the collective weight of the two electrodes with the capacitance and mass of an individual electrode. Nevertheless, the specific capacitance (denoted as C_{sp} in F g^{-1} unit) of the symmetric two-electrode system is computed using the subsequent Equation 9.

$$C_{sp} = \frac{4J\Delta t}{\Delta V} \tag{9}$$

Where *J* is the current density (A g^{-1}).

Charge storage mechanism

Tafel's method

Through CV analysis, insights into the charge storage mechanism can be deduced. Tafel's equation (Equation 10) was utilized for this purpose, and taking the logarithm of both sides yield Equation 11 [2]:

$$I = av^b \tag{10}$$

$$log(I) = b\, log(v) + log(a) \tag{11}$$

Here, *I* represent the working electrode current at $V = 0$ *V*, *v* is the scan rate, and b is the slope. The value of the slope *b* is crucial in determining the charge storage mechanism. A slope *b* equal to 0.5 indicates a Faradic intercalation process, 1 signifies the Electric Double Layer (EDL) capacitance method, and $0.5 < b < 1$ suggests a combination of both techniques [2].

Dunn's approach

To calculate the percentages of capacitive-controlled current and diffusion controlled current in the total produced current during the cyclic voltammetry (CV) scan, Dunn's approach is utilized [2]. Equation 12 provides the capacitive and diffusion-controlled resultant current at a specific scan rate and potential difference.

$$I(V) = k_1 \nu + k_2 \nu^{\frac{1}{2}} \tag{12}$$

$$\frac{I(V)}{\nu^{\frac{1}{2}}} = k_1 \nu^{\frac{1}{2}} + k_2 \tag{13}$$

In Equation 12, $k_1\nu$ denotes the capacitive resultant current, and $k_2\nu^{1/2}$ represents the resulting current in a diffusion-controlled system. By employing Equation 13, both k_1 and k_2 can be determined from the slope and y-intercept of the ($i(V)/\nu^{1/2} \sim \nu^{1/2}$) graph, respectively. In this investigation, the value of current (i) was measured at $V = 0$ V.

Trassatti's approach

The impact of the charge storage technique on the overall capacitance can be examined with Trasatti's approach [2]. From ($1/C_{sp} \sim \nu^{1/2}$) and ($C_{sp} \sim 1/\nu^{1/2}$) graphs, total capacitance (C_T) and EDL capacitance (C_{EDL}) can be determined by taking the y-intercepts using Equation 15 and Equation 17, respectively, and pseudocapacitance (C_{pseu}) from Equation 18.

$$\frac{1}{C_{sp}} = constant \times \nu^{0.5} + \frac{1}{C_T} \tag{14}$$

$$C_T = \frac{1}{y\ intercept\ of \left(\frac{1}{C_{sp}} \sim \nu^{0.5}\right) graph} \tag{15}$$

$$C_{sp} = constant \times \nu^{-0.5} + C_{EDL} \tag{16}$$

$$C_{EDL} = y\ intercept\ of \left(C_{sp} \sim \frac{1}{\nu^{0.5}}\right) graph \tag{17}$$

$$C_{pseudo} = C_T - C_{EDL} \tag{18}$$

$$C_{EDL}(\%) = \frac{C_{EDL}}{C_{sp}} \times 100\% \tag{19}$$

$$C_{pseudo}(\%) = \frac{C_{pseudo}}{C_{sp}} \times 100\% \tag{20}$$

The percentages of C_{EDL} and C_{pseu} in the total capacitance can be calculated from Equation 19 and Equation 20, respectively.

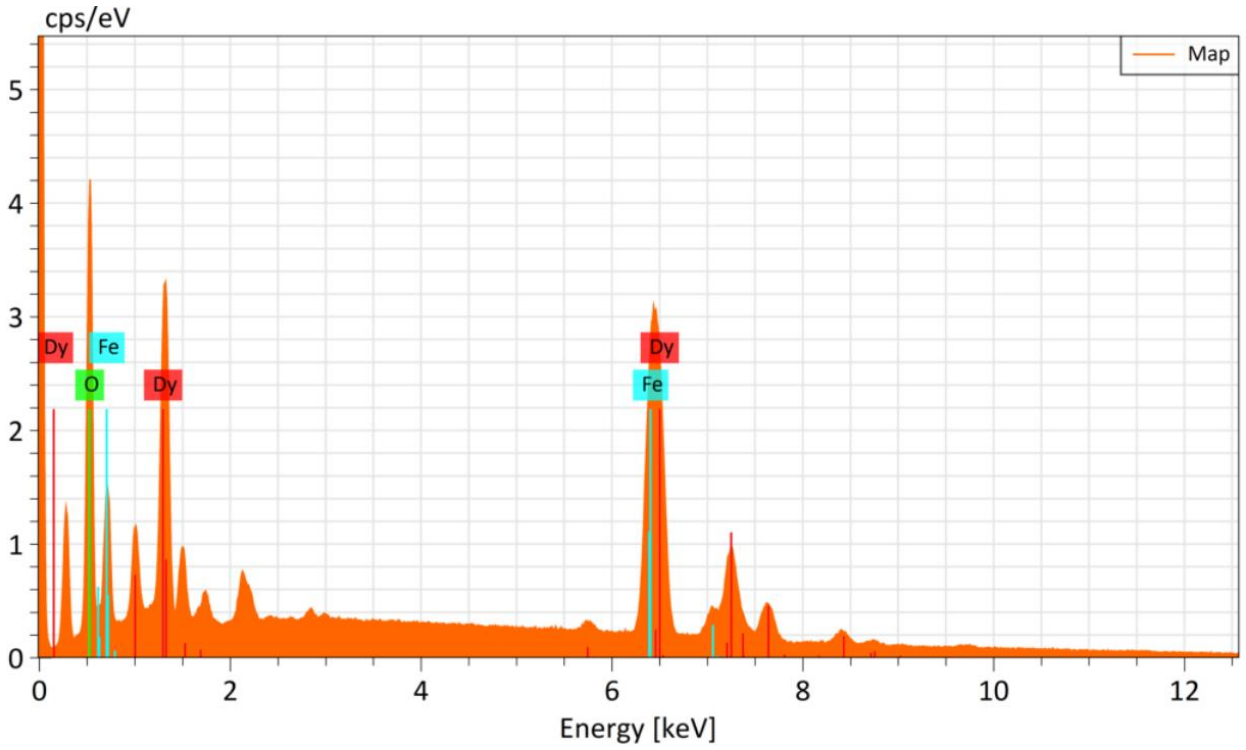

Fig. S4 *EDX spectrum shows the presence of desired atoms (Dy, Fe, and O) in $DyFeO_3$ nanoparticles.*

Table S1 *Mass and atomic percentages of corresponding elements in $DyFeO_3$ nanoparticles as obtained via EDX analysis were consistent with theoretical analysis, which indicates the successful formation of $DyFeO_3$ nanoparticles.*

Elements	Mass (%) (theoretical)	Mass (%) (experimental)	Atom (%) (theoretical)	Atom (%) (experimental)
Dy	61.01	60.97	20	22.97
Fe	20.97	22.42	20	23.60
O	18.02	16.61	60	53.43

Table S2 *The XPS spectrum of $DyFeO_3$ nanoparticles revealed several distinct peaks corresponding to the oxidation states of Dy, Fe and O [3-6]. These oxidation states contribute to the pseudocapacitive charge storage of that nanoparticles.*

Element	**Orbital**	**Peaks**	**Binding energy (eV)**
Dy	Dy 4p	$4p_{3/2}$ (Dy^{4+})	296.26
	Dy 3d	$3d_{5/2}$ (Dy^{3+})	1334.58
		$3d_{3/2}$ (Dy^{3+})	1296.37
Fe	Fe 2p	$2p_{3/2}$ (Fe^{3+})	723.97
		$2p_{3/2}$ (Fe^{2+})	725.99
		$2p_{1/2}$ (Fe^{3+})	710.28
		$2p_{1/2}$ (Fe^{2+})	712.58
		satellite	718.77
	Fe 3p	Fe^{3+}	56.01
		Fe^{2+}	54.83
O	O 1s	O^{2-}	529.53
		Satellite (oxygen vacancies)	531

Table S3 *Comparison of various properties of commonly used electrolytes in energy storage devices. This comparison suggests that Na_2SO_4 is one of the best choices as an electrolyte material in terms of ion size, conductivity, and price.*

Electrolyte	Ion	Bare ion size (Å)	Hydrated ion size (nm)	Ionic conductivity (S cm^2 mol^{-1}) (aq.)	Conductivity (mS cm^2)	Price ($ g^{-1})	CAS no.
Na_2SO_4	Na^+	0.095	0.358	50.11	91.1	0.02	7757-82-6
	SO_4^{2-}	0.290	0.379	160			
LiTFSI	Li^+	0.060	0.382	38.69	2.7	6.37	90076-65-6
	$(CF_3SO_2)_2N^-$	0.0325		14.40 (PC)			
$LiSO_4$	Li^+	0.060	0.382	38.69	-	0.33	10377-48-7
	SO_4^{2-}	0.290	0.379	160			
$NaNO_3$	Na^+	0.095	0.358	50.11	80	0.14	7631-99-4
	NO_3^-	0.264	0.335	71.42			
$NaClO_4$	Na^+	0.095	0.358	50.11	75	0.33	7601-89-0
	ClO_4^-	0.292	0.338	67.3			
KOH	K^+	1.33	0.331	73.5	540	0.03	1310-58-3
	OH^-	0.176	0.3	198			

Based on the data presented in Table S3, it can be asserted that Na_2SO_4 and KOH emerge as optimal electrolyte choices, considering factors such as hydrated ion size, ionic conductivity, and price. However, it is important to note that despite its favorable properties, KOH is a corrosive substance, potentially compromising the longevity of energy storage devices and promoting undesirable side reactions. In contrast, Na_2SO_4, being a neutral substance, avoids such issues, thereby enhancing the durability of the energy storage system. In our investigation, we selected a significantly low concentration of Na_2SO_4 as the electrolyte exploring the inherent advantages of Na_2SO_4.

Table S4 *The comparison of different properties among frequently employed solvent media in electrolyte solutions for energy storage devices indicates that acetonitrile emerges as a prime selection for aqueous-based SEI (solid electrolyte interface) owing to its favorable attributes such as reduced viscosity, high dielectric constant, and economical pricing.*

Solvent	Dielectric constant (ε)	Viscosity (mPa s^{-1})	Conductivity (μ S m^{-1})	Melting point (°C)	Boiling point (°C)	Price ($ ml^{-1})	CAS no.
Water	80.1	1.0016	0.05	0	100	-	-
Ethanol	24.3	1.07	1.35×10^{-13}	-117.3	78.5	0.03	64-17-5
Acetonitrile	36.6	0.37	6×10^{-4}	-46	82	0.05	75-05-8
Ethylene glycol	37	2.2	0.2	-13	195	0.09	107-21-1

Electrochemical evaluation in three-electrode system

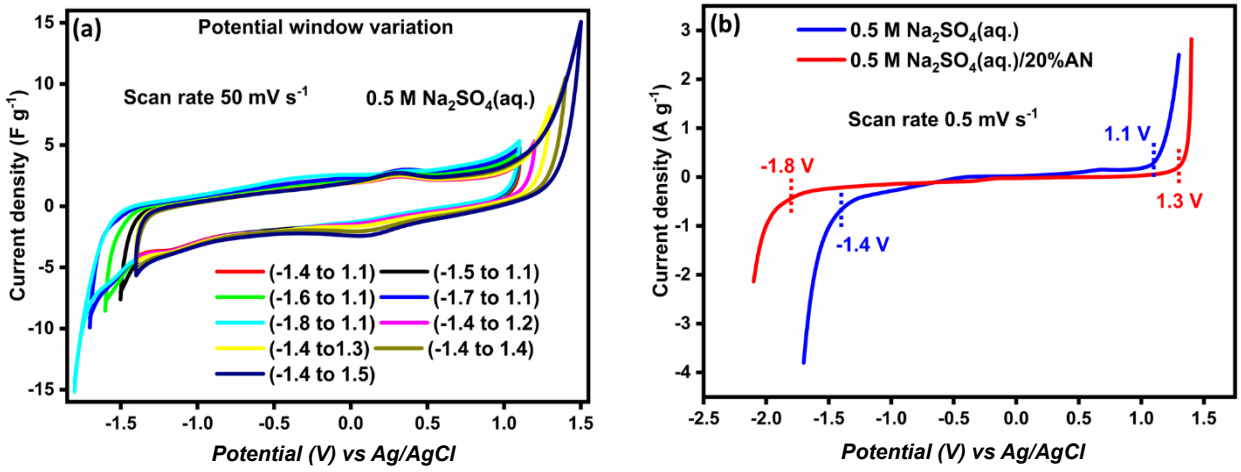

Fig. S5 ***(a)*** *The potential window of the $DyFeO_3$ electrode material across different ranges in a 0.5 M Na_2SO_4(aq.) electrolyte solution, maintaining a constant scan rate of 50 mV s^{-1}. From the range of potential windows assessed, the interval from -1.4 to 1.1 V was selected for subsequent electrochemical investigations.* ***(b)*** *LSV curves demonstrate that the water oxidation potential of the $DyFeO_3$ electrode material in 0.5 M Na_2SO_4(aq.) and 0.5 M Na_2SO_4(aq.)/20%AN electrolyte solutions at the scan rate of 0.5 mV s^{-1} exceeds the theoretical water oxidation potential (1.23 V).*

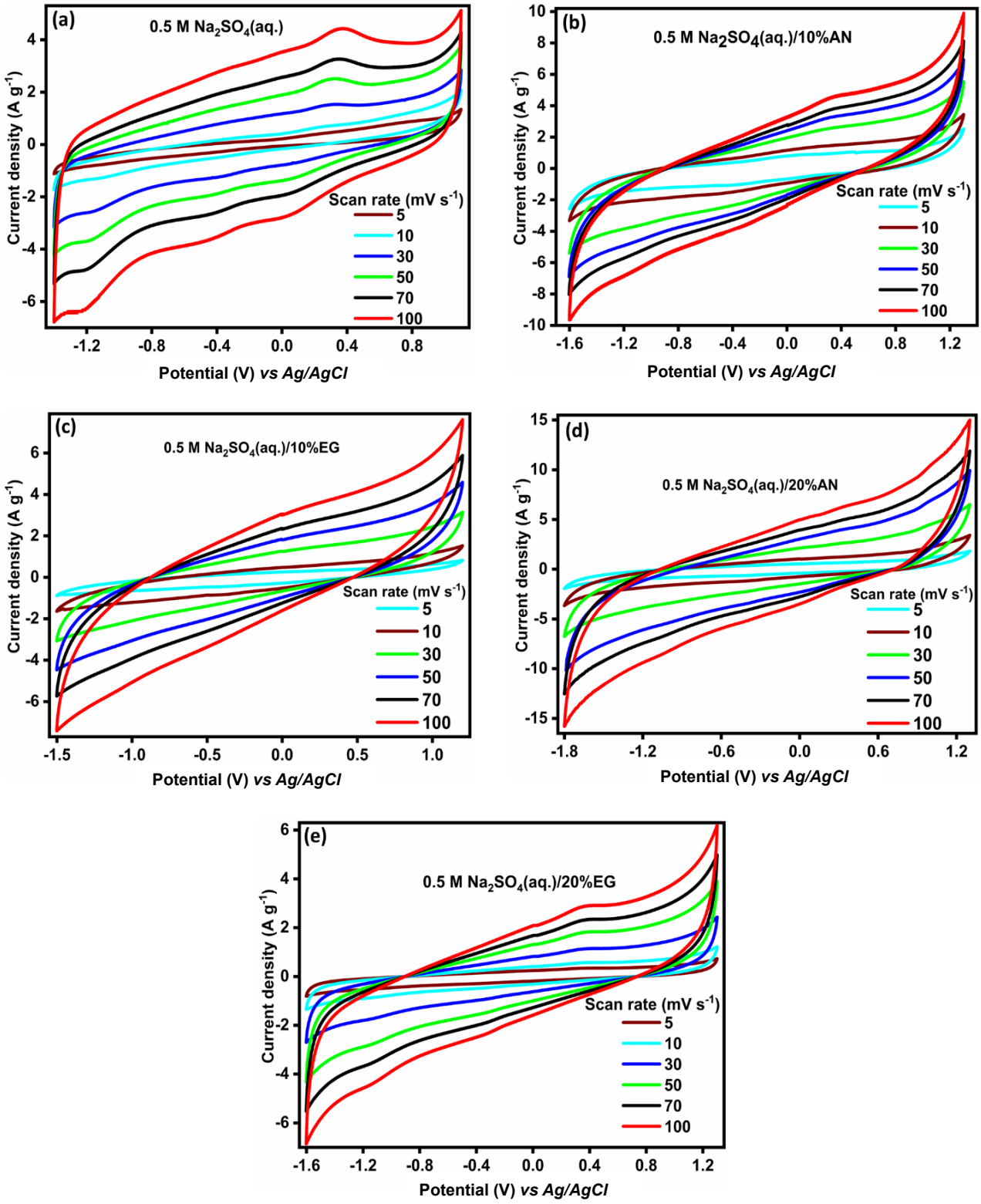

Fig. S6 *CV curves of $DyFeO_3$ electrode material in* ***(a)*** *0.5 M Na_2SO_4(aq.),* ***(b)*** *0.5 M Na_2SO_4(aq.)/10%AN,* ***(c)*** *0.5 M Na_2SO_4(aq.)/10%EG,* ***(d)*** *0.5 M Na_2SO_4(aq.)/20%AN and* ***(e)*** *0.5 M Na_2SO_4(aq.)/20%EG electrolytic solutions. All the CV curves demonstrate that, with increasing scan rate the integrated CV area also increases and the shape of the curves remains unchanged within the ultra-high potential window (2.5 to 3.1 V).*

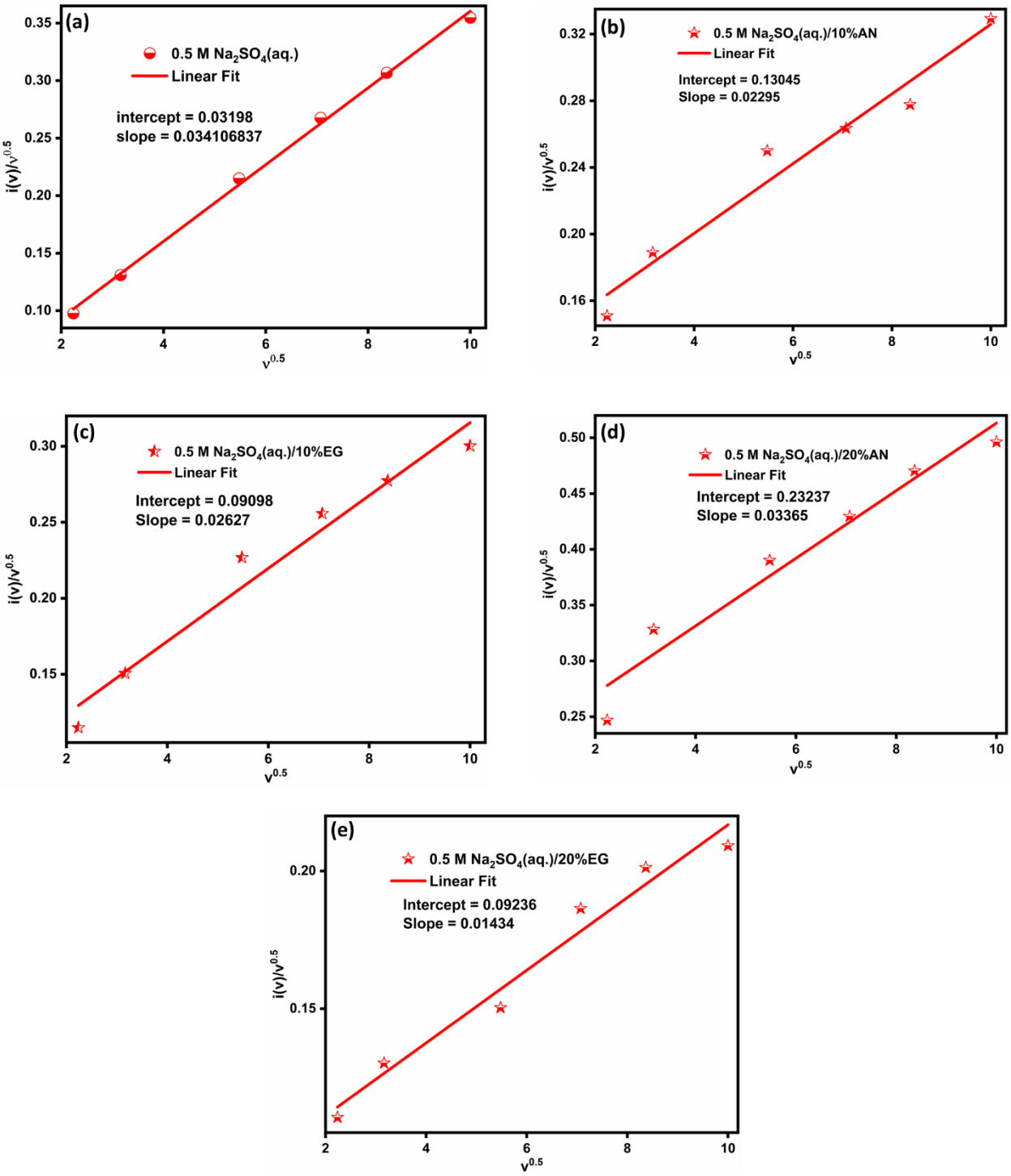

Fig. S7 *The* $(\frac{i(V)}{\nu^{\frac{1}{2}}} \sim \nu^{\frac{1}{2}})$ *graph for the* $DyFeO_3$ *electrode material in* ***(a)*** *0.5 M* Na_2SO_4*(aq.),* ***(b)*** *0.5 M* Na_2SO_4*(aq.)/10%AN,* ***(c)*** *0.5 M* Na_2SO_4*(aq.)/10%EG,* ***(d)*** *0.5 M* Na_2SO_4*(aq.)/20%AN and* ***(e)*** *0.5 M* Na_2SO_4*(aq.)/20%EG electrolytic solutions. By incorporating the y-intercept and slope values obtained from these graphs into Dunn's equation, we computed the percentages of capacitive-controlled current and diffusion-controlled current.*

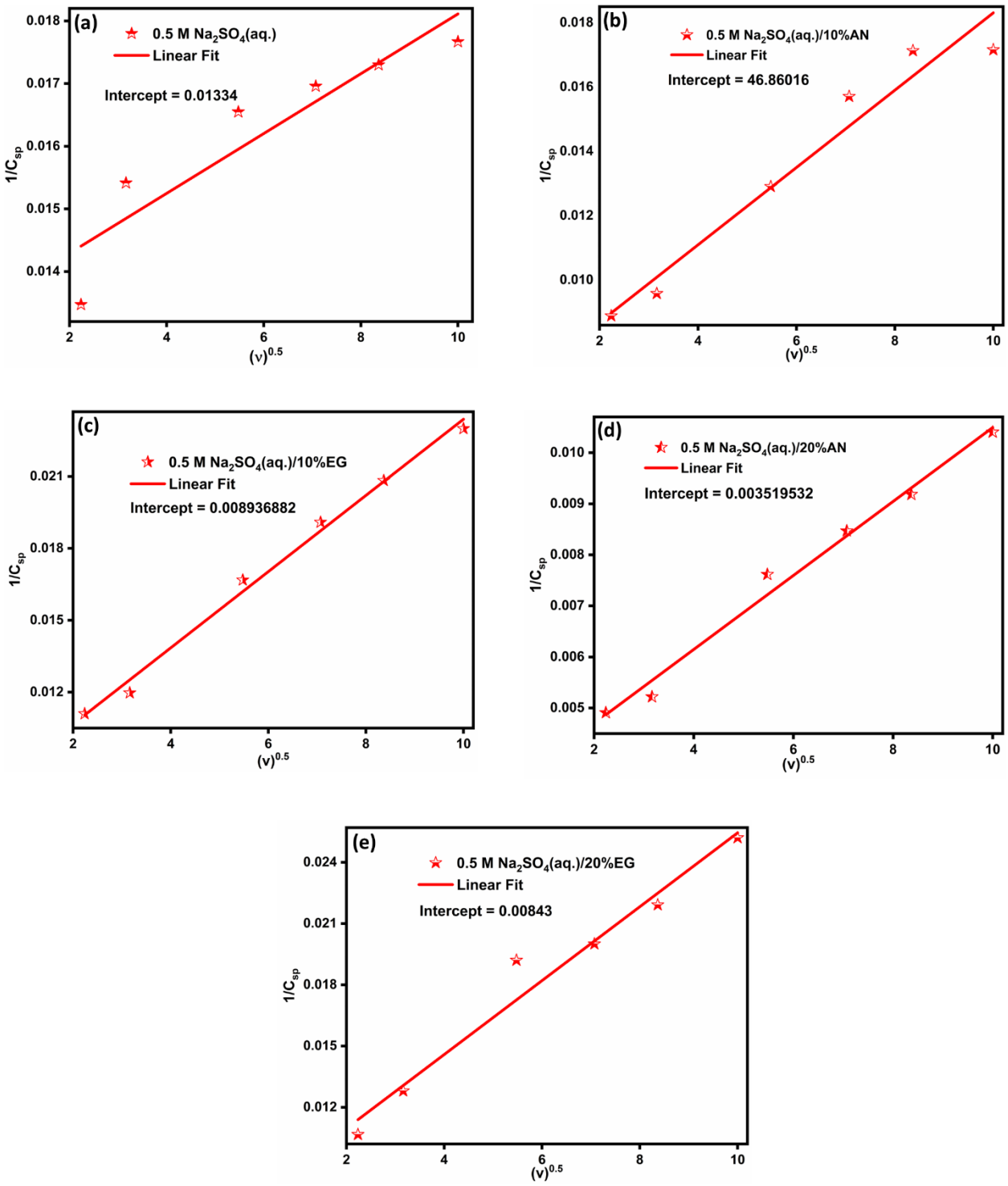

Fig. S8 ***(a)*** *The* $\frac{1}{C_{SP}} \sim v^{\frac{1}{2}}$ *graph for the* $DyFeO_3$ *electrode material in* ***(a)*** *0.5 M* Na_2SO_4*(aq.),* ***(b)*** *0.5 M* Na_2SO_4*(aq.)/10%AN,* ***(c)*** *0.5 M* Na_2SO_4*(aq.)/10%EG,* ***(d)*** *0.5 M* Na_2SO_4*(aq.)/20%AN and* ***(e)*** *0.5 M* Na_2SO_4*(aq.)/20%EG electrolytic solutions. By incorporating the y-intercept values obtained from these graphs into Trassatti's equation, we computed the value of total capacitance (*C_T*).*

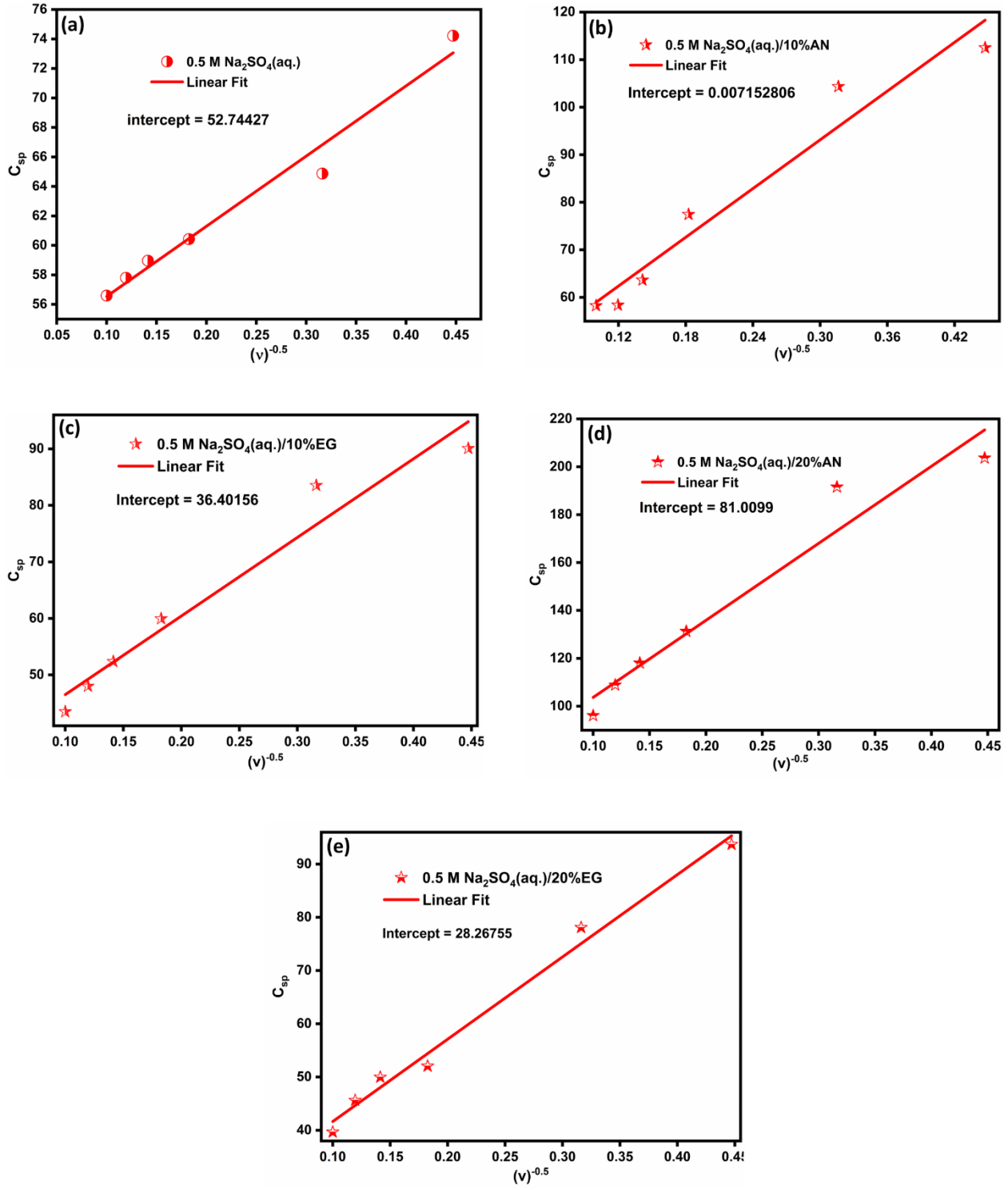

Fig. S9 *The $C_{sp} \sim v^{-\frac{1}{2}}$ graph for the $DyFeO_3$ electrode material in* ***(a)*** *0.5 M Na_2SO_4(aq.),* ***(b)*** *0.5 M Na_2SO_4(aq.)/10%AN,* ***(c)*** *0.5 M Na_2SO_4(aq.)/10%EG,* ***(d)*** *0.5 M Na_2SO_4(aq.)/20%AN and* ***(e)*** *0.5 M Na_2SO_4(aq.)/20%EG electrolytic solutions. By incorporating the y-intercept values obtained from these graphs into Trassatti's equation, we computed the value of EDL capacitance (C_{EDL}).*

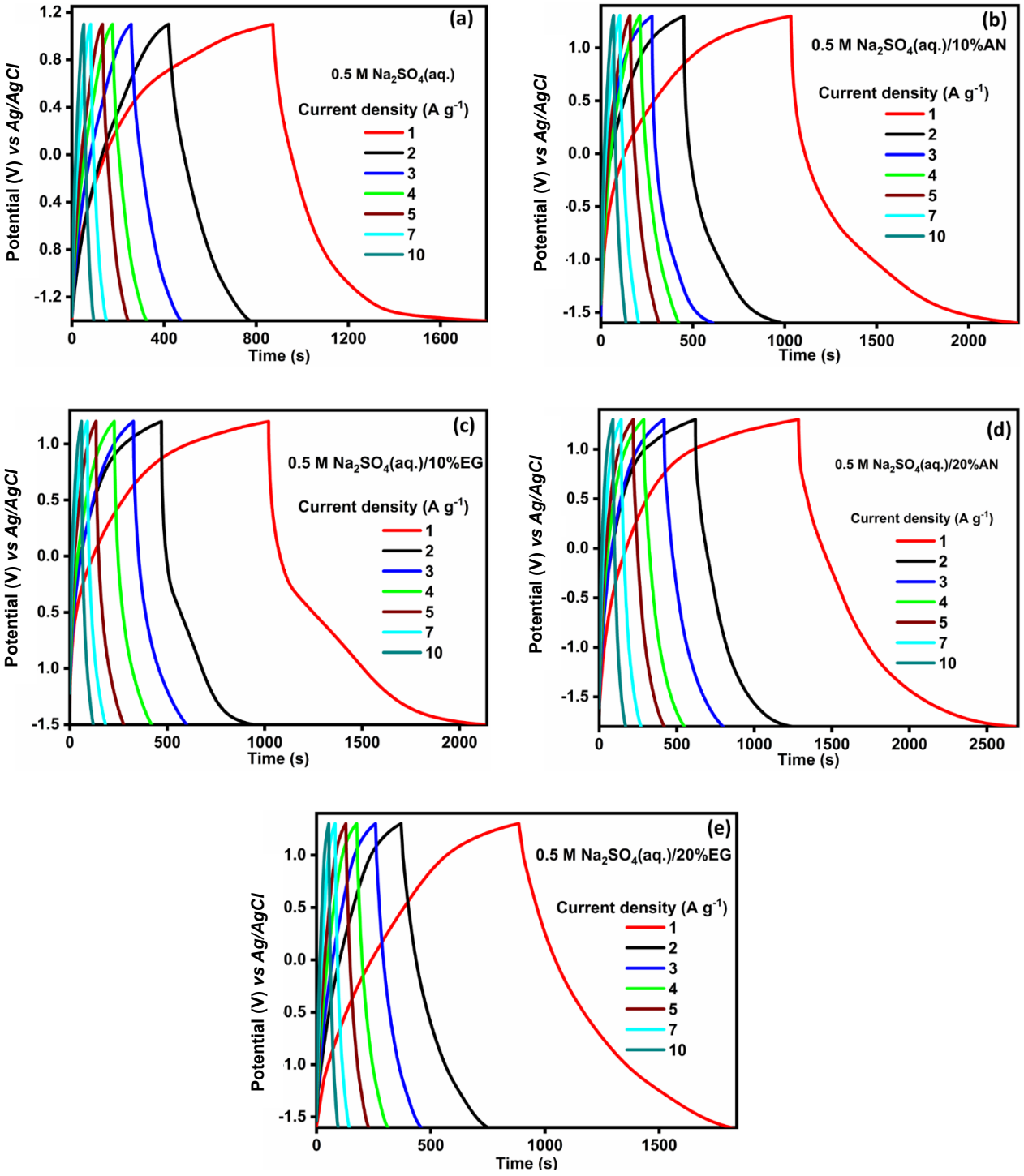

Fig. S10 *GCD curves of $DyFeO_3$ electrode material in* ***(a)*** *0.5 M Na_2SO_4(aq.),* ***(b)*** *0.5 M Na_2SO_4(aq.)/10%AN,* ***(c)*** *0.5 M Na_2SO_4(aq.)/10%EG,* ***(d)*** *0.5 M Na_2SO_4(aq.)/20%AN and* ***(e)*** *0.5 M Na_2SO_4(aq.)/20%EG electrolytic solutions. All the GCD curves demonstrate that, with increasing current density the charge/discharge durations also decrease.*

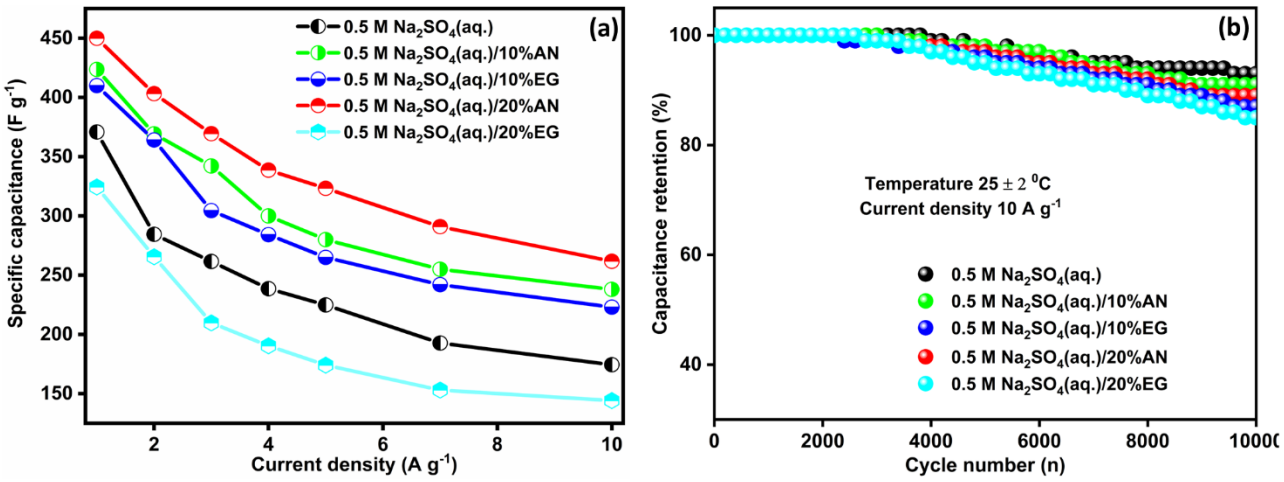

Fig. S11(a) *The variation of C_{sp} with increasing current densities demonstrates the superior charge storage capacity of the $DyFeO_3$ electrode material across different electrolyte solutions. Notably, among these solutions, the $DyFeO_3$ electrode material attains the highest capacitance value in the 0.5 M Na_2SO_4(aq.)/20%AN electrolyte.* ***(b)*** *the specific capacitance retention at a constant current density of 10 A g^{-1} and room temperature is presented. $DyFeO_3$ exhibits exceptionally high capacitance retention across diverse electrolyte solutions. Notably, in the 0.5 M Na_2SO_4(aq.)/20%AN electrolyte solution, $DyFeO_3$ demonstrates the highest capacitance retention, highlighting its superior performance in this specific electrolytic environment.*

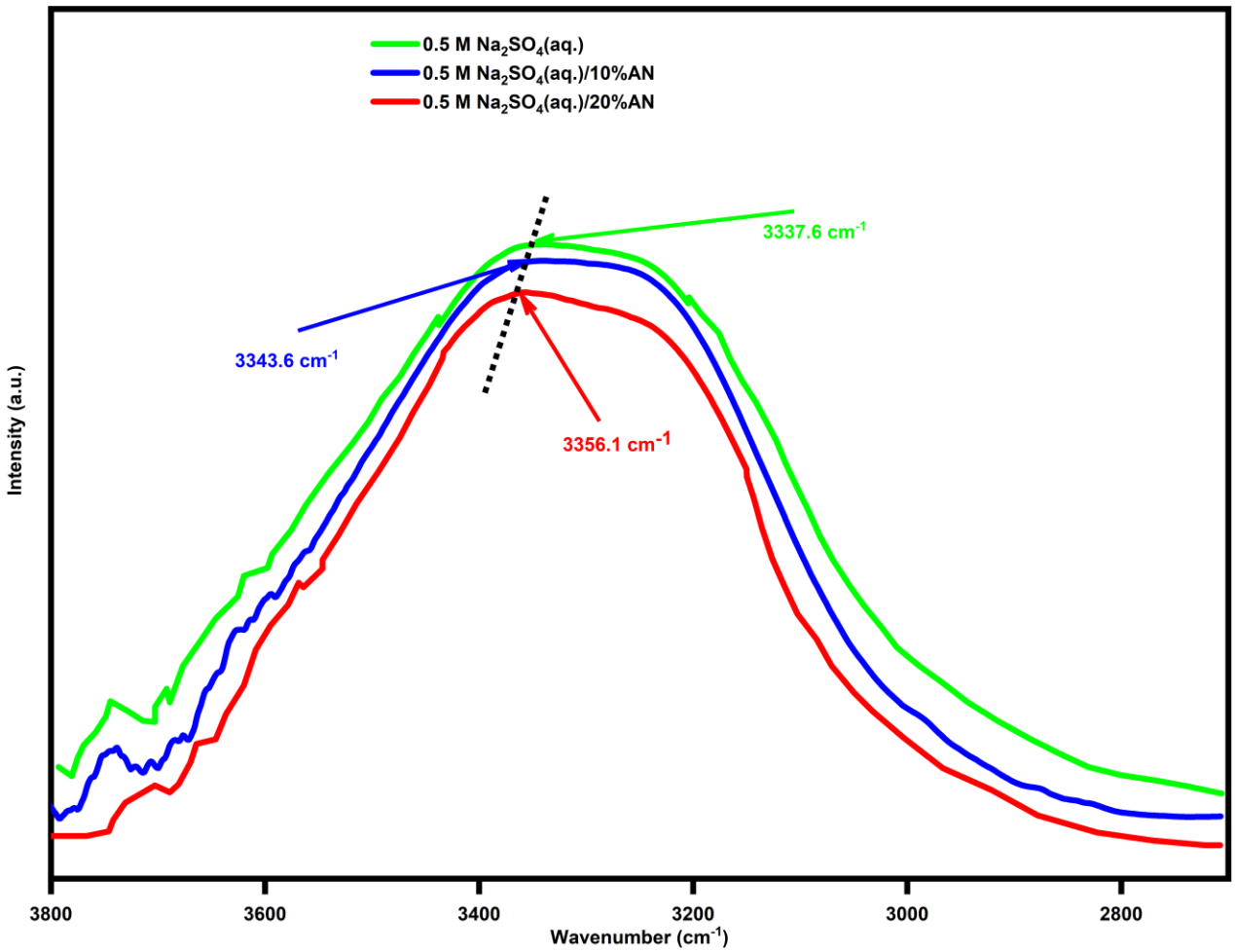

Fig. S12 *The prominent peak observed at 3337.6 cm^{-1} in the FTIR spectra of the electrolyte solution comprising AN with 0.5 M Na_2SO_4(aq.) corresponds to the H-bending vibrational mode of water molecules. This peak shifts as the concentration of AN increases, consequently impeding the unrestricted mobility of water molecules.*

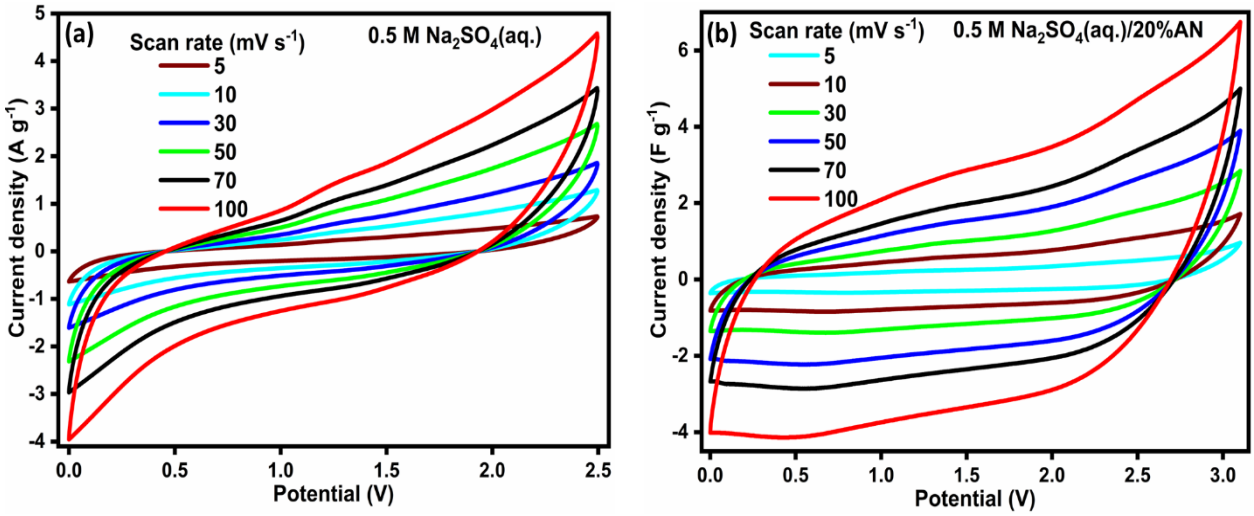

Fig. S13 *CV curves of $DyFeO_3$ electrode material in* ***(a)*** *0.5 M Na_2SO_4(aq.), and* ***(b)*** *0.5 M Na_2SO_4(aq.)/20%AN electrolyte solution. All the CV curves demonstrate that, with increasing scan rate the integrated CV area also increases and the shape of the curves remains unchanged within the ultra-high potential window (2.5 to 3.1 V).*

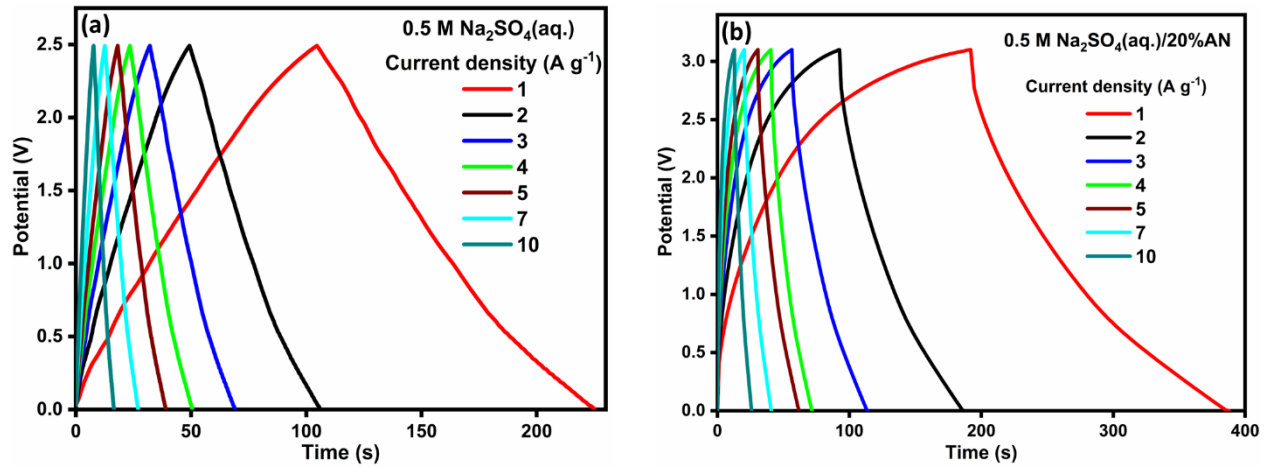

Fig. S14 *GCD curves of $DyFeO_3$ electrode material in* ***(a)*** *0.5 M Na_2SO_4(aq.), and* ***(b)*** *0.5 M Na_2SO_4(aq.)/20%AN electrolyte solution. All the GCD curves demonstrate that the charge/discharge durations decrease with increasing current density.*

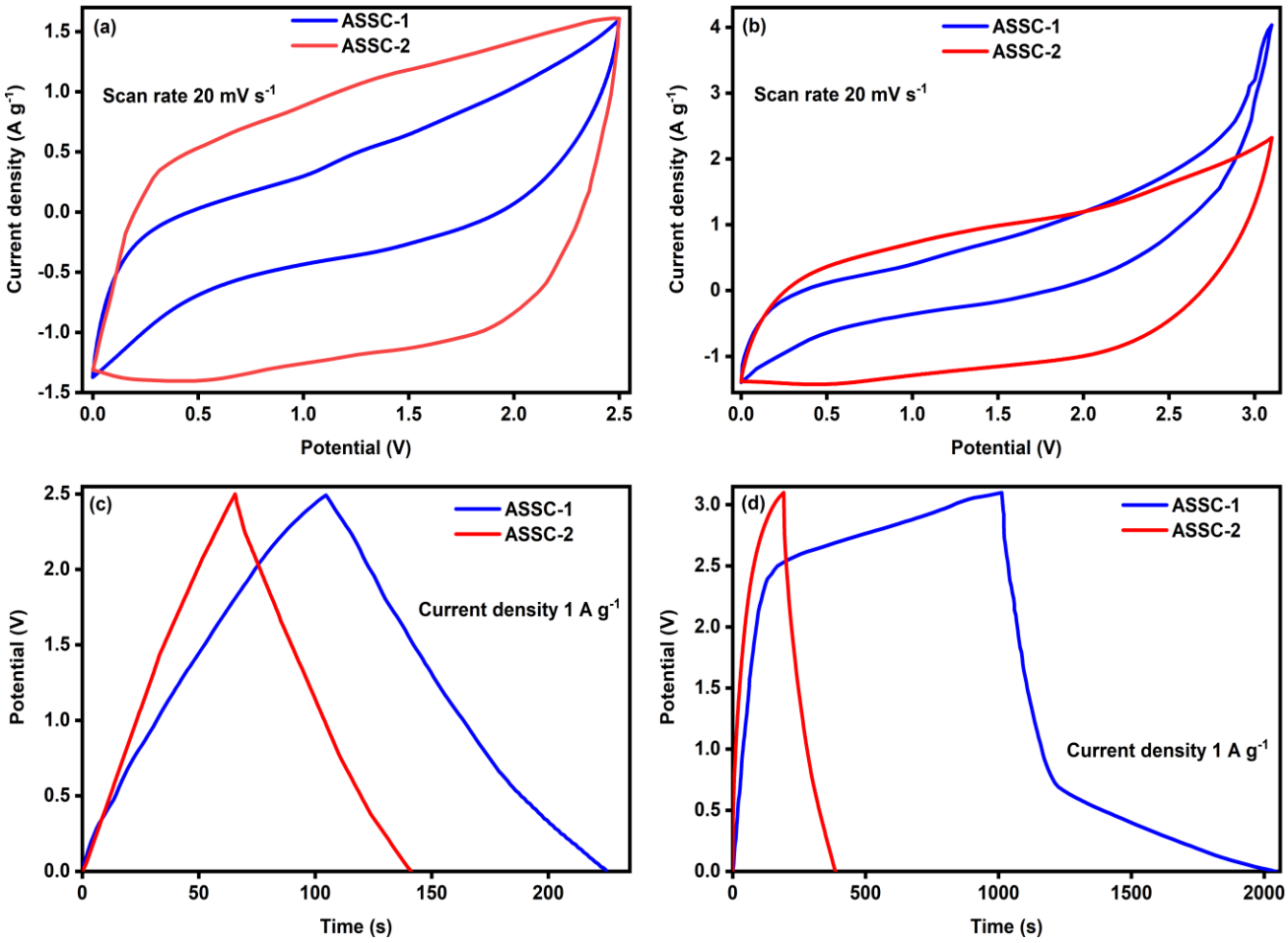

Fig. S15 *CV and GCD analysis of ASSC-1 and ASSC-2 at different cutoff potentials. (a, b) CV curves of ASSC-1 and ASSC-2 at a scan rate of 20 mV s^{-1}, measured at cutoff potentials of 2.5 V and 3.1 V, respectively. ASSC-1 shows a pronounced increase in current density at 3.1 V, indicating significant gas evolution due to water decomposition, while ASSC-2 exhibits stable current density, demonstrating the effect of acetonitrile in suppressing water electrolysis. (c, d) GCD curves of ASSC-1 and ASSC-2 at a current density of 1 A g^{-1} for cutoff potentials of 2.5 V and 3.1 V, respectively. The non-linear potential drop observed in ASSC-1 at 3.1 V suggests gas formation and increased internal pressure within the cell. In contrast, ASSC-2 shows stable potential profiles at both potentials, highlighting acetonitrile's role in mitigating gas evolution by reducing the activity of free water molecules.*

Table S5 *A comparative analysis of self-discharge and leakage current of aqueous based supercapacitors.*

Electrode material	Electrolyte	Cell potential	Self-discharge voltage (floating time)	Leakage current (holding time)	Ref.
Activated carbon//Zn	3 M $ZnSO_4$	1.8 V	0.55 V (60 h)	11 mA g^{-1} (50 h)	[7]
Ti_3/α-MnO_2	CH_3COOK+LITFSI	2.2 V	0.8 V (14 h)	5.5 mA g^{-1} (25 h)	[8]
Activated carbon//Activated carbon	2 M $ZnSO_4$	1.8 V	0.99 V (10 h)	-	[9]
Carbon//Carbon	1 M $LiSO_4$	2.5 V	-	8 mA g^{-1} (2 h)	[10]
$DyFeO_3$//$DyFeO_3$	0.5 M Na_2SO_4(aq.)/20%AN	3 V	0.55 V (60 h)	6.71 mAg^{-1} (50 h)	This work

Table S6 *A comparative analysis of production costs for different hybrid-type electrolyte systems (per 100 ml) was conducted utilizing the prices outlined in* ***Table S3*** *and* ***Table S4****.*

Electrolytes	Price ($ 100 ml^{-1})
1 M Na_2SO_4/H_2O	0.28
1 M $NaClO_4/H_2O$/95%ACN	8.79
17 m $NaClO_4/H_2O$	68.69
1 M Na_2SO_4/H_2O/50%EG	4.78
0.5 M Na_2SO_4 (aq.)	0.14
0.5 M Na_2SO_4 (aq.)/20%AN	1.14

The cost analysis of electrolyte solutions presented in Table S6 is derived from the pricing data of diverse electrolytes outlined in Table S3 and various electrolyte media in Table S4. Evaluation of the aforementioned electrolyte solution prices indicates that 0.5 M Na_2SO_4(aq.) as a 100% aqueous electrolyte and 0.5 M Na_2SO_4(aq.)/20%AN as an aqueous electrolyte incorporating organic additives stand out as the most optimal choices for supercapacitor applications. Adopting these electrolyte solutions not only aligns with superior performance but also effectively minimizes the overall manufacturing expenses associated with energy storage devices.

Table S7 Crystallographic *parameters of the as-synthesized $DyFeO_3$ nanoparticles before and after 10000 GCD cycles obtained after Rietveld refinement. Analysis of the XRD data suggests that this material maintained its structural integrity without undergoing any phase transformation making our synthesized nanoparticles a reliable electrode material for symmetric hybrid supercapacitors.*

Parameters	Before 10000 GCD cycles	After 10000 GCD cycles
Crystallographic phase	Orthorhombic	Orthorhombic
Space group	*Pnma*	*Pnma*
a (Å)	5.59324	5.59390
b (Å)	7.62289	7.62165
c (Å)	5.30227	5.30239
Volume V (Å^3)	226.071036	226.066080
$\alpha = \beta = \gamma$ (*d*egree)	90	90
d-spacing (nm)	2.70794	2.70781
Crystallinity (%)	93.47	83.7
Goodness of fit χ^2	2.1	2.5

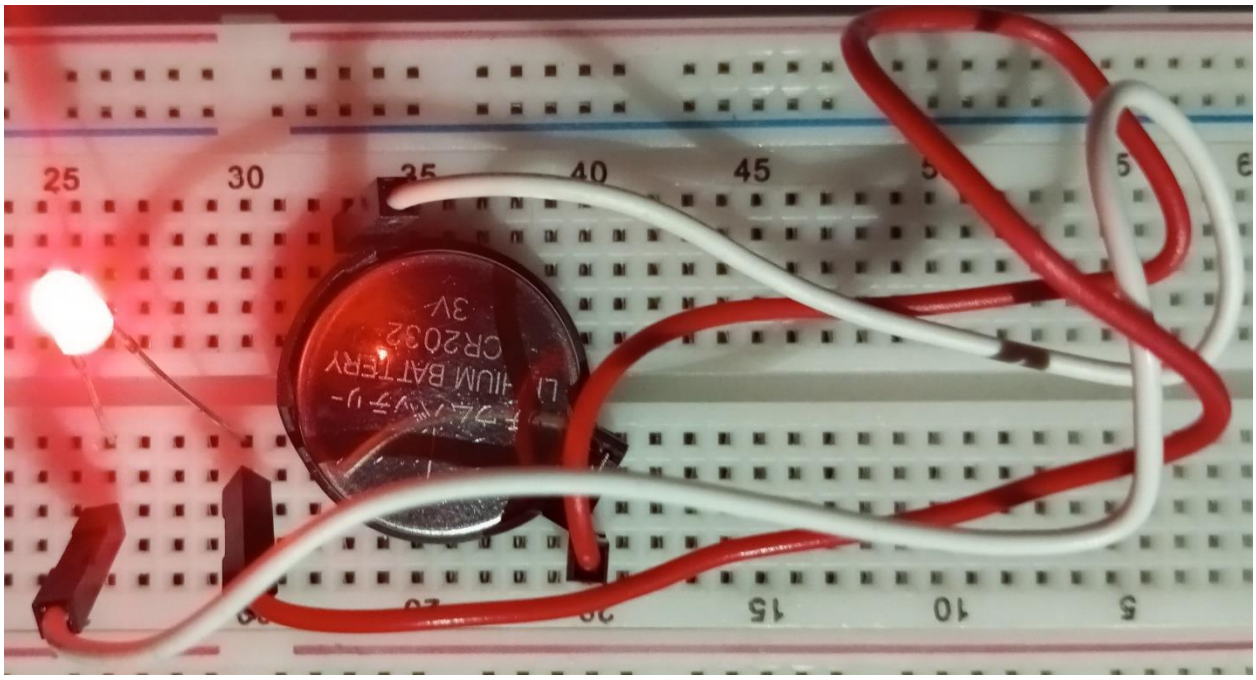

Fig. S16 *A real-world showcase of our fabricated coin cell supercapacitor in symmetric configurations employing $DyFeO_3$ nanoparticles as the electrode substance and a 0.5 M Na_2SO_4(aq.)/20%AN solution as the electrolyte. The successful lighting up of an LED by this coin-cell supercapacitor demonstrates its practical utility.*

References

1. S. A. Melchior, K. Raju, I. S. Ike, R. M. Erasmus, G. Kabongo, I. Sigalas, S. E. Iyuke and K. I. Ozoemena, *J. Electrochem. Soc.*, 2018, **165**, A501–A511.
2. M. Tarek and M. A. Basith, *J. Mater. Chem. C*, 2023, **11**, 16605–16622.
3. X. Liu, J. You, R. Wang, Z. Ni, F. Han, L. Jin, Z. Ye, Z. Fang and R. Guo, *Sci. Rep.*, 2017, **7**, 13085.
4. K. A. Owusu, L. Qu, J. Li, Z. Wang, K. Zhao, C. Yang, K. M. Hercule, C. Lin, C. Shi, Q. Wei et al., *Nat. Commun.*, 2017, **8**, 14264.
5. D.-Q. Yang and E. Sacher, *J. Mater. Chem. C*, 2009, **113**, 6418–6425.
6. R. Liu, Z. Wang, S. Peng, J. Bi, J. Wu and Z.-G. Ye, *J. Am. Ceram. Soc.*, 2020, **103**, 1097–1104.
7. J. N. Ramavath, M. Raja, K. Balakumar and R. Kothandaraman, *J. Electrochem. Soc.*, 2021, **168**, 010538.
8. H. Avireddy, B. W. Byles, D. Pinto, J. M. D. Galindo, J. J. Biendicho, X. Wang, C. Flox, O. Crosnier, T. Brousse, E. Pomerantseva et al., *Nano Energy*, 2019, **64**, 103961.
9. J. Yang, M. A. Bissett and R. A. Dryfe, *ChemSusChem*, 2021, **14**, 1700–1709.
10. 81 J. N. Ramavath, S. Potham and K. Ramanujam, *J. Electrochem. Soc.*, 2021, **168**, 070538.